

Stochastic bifurcations in a vibro-impact Duffing–Van der Pol oscillator

Pankaj Kumar · S. Narayanan · Sayan Gupta

Received: 6 August 2015 / Accepted: 21 February 2016 / Published online: 15 March 2016
© Springer Science+Business Media Dordrecht 2016

Abstract The stochastic bifurcations in a vibro-impact Duffing–Van der Pol oscillator, subjected to white noise excitations, are investigated. Bifurcations in noisy systems occur either due to topological changes in the phase space—known as D-bifurcations—or due to topological changes associated with the stochastic attractors—known as P-bifurcations. In either case, the singularities in the phase space near the grazing orbits due to impact lead to inherent difficulties in bifurcation analysis. Loss of dynamic stability—or D-bifurcations—is analyzed through computation of the largest Lyapunov exponent using the Nordmark–Poincare mapping that enables bypassing the problems associated with discontinuities. For P-bifurcation analysis, the steady-state solution of the Fokker–Planck equation is computed after applying suitable non-smooth coordinate transformations and mapping the problem into a continuous domain. A quantitative measure for P-bifurcations has been carried out using a newly developed mea-

sure based on Shannon entropy. A comparison of the stability domains obtained from P-bifurcation and D-bifurcation analyses is presented which reveals that these bifurcations need not occur in same regimes.

Keywords Vibro-impact · Duffing–Van der Pol oscillator · Zhuravlev–Ivanov transformation · Nordmark–Poincare mapping · Shannon entropy · Stochastic bifurcation

1 Introduction

Vibro-impact dynamical systems are common in applications that involve moving parts connected with motion-limiting stops, such as joints, gears, and systems with sliding contacts. The dynamics of such systems are complex because of the nonlinearities induced on the system on account of impact [17, 18] and exhibit rich phenomenological behavior, such as grazing bifurcation [7], torus bifurcation [25], and chatter and sticking [34]. The presence of noise in the excitations leads to further complexities in the dynamical behavior of these systems. Noise has the potential to alter the boundaries of the stability regimes, the state-space characteristics, and their basins of attractions, especially in multistable systems [1, 22]. This has led to recent focus on analyzing the behavior of vibro-impact systems under stochastic loadings [6, 10, 12–14, 31, 39]. Methods based on stochastic averaging have been used extensively for these studies; see [11, 13, 14, 16, 33]. However, the applicability of stochastic aver-

P. Kumar
Department of Mechanical Engineering, Indian Institute of Technology Madras, Chennai 600036, India

S. Narayanan
Indian Institute of Information Technology (Design and Manufacturing) Kancheepuram, Chennai 600127, India

S. Gupta (✉)
Department of Applied Mechanics, Indian Institute of Technology Madras, Chennai 600036, India
e-mail: gupta.sayan@gmail.com

aging methods is limited to small noise intensities, small values of damping, and coefficient of restitution being close to unity. Monte Carlo simulation-based approaches are applicable under more general settings and have been used for studying vibro-impact systems in [19], but are computationally expensive. The method of multiple scales has been adopted in [31] to obtain the stationary probability density function (pdf) of the response of vibro-impact systems. The pdf of the responses of vibro-impact systems have been obtained from the solution of the corresponding Fokker–Planck (FP) equation in [39]. Here, the authors use the exponential polynomial closure method for obtaining the marginal pdf of the response of vibro-impacting system.

The focus of this study is to carry out a stochastic bifurcation analysis of a vibro-impact Duffing–Van der Pol (DVDP) oscillator subjected to white noise excitations. The analysis is carried out using two distinct approaches. Changes in the dynamical stability of the system are examined through the largest Lyapunov exponent (LLE) associated with the trajectories of the system. In computing the LLE, the discontinuities in the equation of motion on account of impact present difficulties which are bypassed by using the Nordmark–Poincare mapping [7, 27]. A change in the sign of LLE is indicative of dynamical or D-bifurcation. Additionally, topological changes associated with the stochastic attractors can take place at different parameter regimes and have a bearing on the attractor space associated with these systems. These changes are characterized as phenomenological or P-bifurcations and involves studying the long-term steady-state pdf of the response state variables, which could be obtained as solutions of the FP equation. The difficulties in writing the FP equation associated with the vibro-impact system whose governing equations of motion are discontinuous are addressed by using the Zhuravlev–Ivanov transformation [9, 20, 40]. A numerical solution to the FP equation in the transformed space is obtained using a recently developed finite element method [23]. Subsequently, a measure based on the Shannon entropy [24] is used to quantify the regimes where P-bifurcations take place.

2 Problem statement

The equations of motion for a DVDP vibro-impact oscillator, with an unilateral zero offset barrier (see Fig.

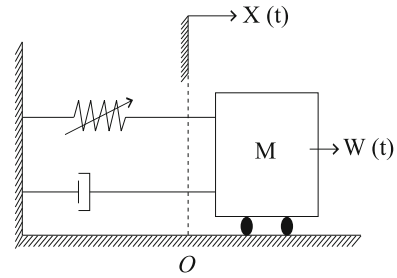


Fig. 1 Schematic of the vibro-impact system with unilateral zero offset barrier

1 for a schematic), subjected to Gaussian excitation are of the form

$$\ddot{X} - \alpha X - c\dot{X} + \beta_0 X^3 - \beta_1 X^2 \dot{X} + \beta_2 X^4 \dot{X} = \sigma W(t), \quad X > 0, \tag{1}$$

subject to the condition

$$\dot{X}^+ = -e\dot{X}^-, \quad X = 0, \quad 0 < e \leq 1. \tag{2}$$

Here, α and c denote the linear stiffness; damping terms $\{\beta_i(t)\}_{i=0}^2$ are system parameter constants that define the nonlinear stiffness and damping; $W(t)$ is a stationary, zero-mean Gaussian process; σ represents its intensity; X , \dot{X} , and \ddot{X} are, respectively, the system displacement, velocity, and acceleration; and e is the coefficient of restitution. This study carries out a stochastic stability analysis for this system, when subjected to white noise excitations and focusses on identifying the stability regimes in the parameter space.

Equation (2) represents the rebound condition of instantaneous impact, where $\dot{X}^- = \dot{X}(t^* - 0)$ is the velocity just before the instant of impact t^* and $\dot{X}^+ = \dot{X}(t^* + 0)$ indicates the rebound velocity. The restitution coefficient $e \leq 1$ is indicative of the energy loss upon impact. For a perfectly elastic impact with zero energy loss, $e = 1$ and \dot{X}^+ and \dot{X}^- have equal magnitudes but are of opposite signs. Equations (1–2) represent a set of coupled equations with discontinuity at $X = 0$. This singularity at the grazing condition presents analytical as well as computational difficulties in subsequent stochastic bifurcation analyses. These difficulties can be bypassed by adopting non-smooth transformations on the state variables and modeling the system in the transformed space. This is discussed in the following section.

3 Non-smooth coordinate transformations

3.1 Zhuravlev transformation

The discontinuity in Eqs. (1–2) can be removed by invoking the mirror image transformation of state variables proposed by Zhuravlev [40]. This involves defining a set of new state variables, given by

$$\begin{aligned} X &= X_1 = |Y| = Y \operatorname{sgn}(Y), & \dot{X} &= X_2 = \dot{Y} \operatorname{sgn} Y, \\ \ddot{X} &= \ddot{Y} \operatorname{sgn} Y. \end{aligned} \tag{3}$$

Here, $\operatorname{sgn}(\cdot)$ represents the *signum* function, such that

$$\operatorname{sgn}(Y) = \begin{cases} 1 & \text{if } Y > 0; \\ -1 & \text{if } Y < 0. \end{cases} \tag{4}$$

The Zhuravlev transformation maps the domain $X > 0$ of the original phase plane (X, \dot{X}) onto the whole phase plane (Y, \dot{Y}) . When Eq. (3) is introduced in Eqs. (1–2) and using the property $(\operatorname{sgn}(Y))^2 = 1$, the transformed equation of motion in the (Y, \dot{Y}) -phase plane can be written as

$$\begin{aligned} \ddot{Y} - \alpha Y - c\dot{Y} + \beta_0 Y^3 - \beta_1 Y^2 \dot{Y} + \beta_2 Y^4 \dot{Y} \\ = \sigma \operatorname{sgn}(Y) W(t), \quad t \neq t^*, \end{aligned} \tag{5}$$

$$\dot{Y}^+ = e\dot{Y}^-, \quad t = t^*. \tag{6}$$

Here, Eq. (6) is a constraint equation. Clearly, at $t = t^*$, there is a discontinuity in the velocity due to the impact when $e \neq 1$. The change in the velocity when $Y(t^*) = 0$ (at impact) is given by

$$(\dot{Y}^- - \dot{Y}^+) \delta(t - t^*) = (1 - e)\dot{Y} \delta(t - t^*), \tag{7}$$

provided $|\dot{Y}^+| < |\dot{Y}| < |\dot{Y}^-|$. Since $Y(t) \approx Y(t^*) + \dot{Y}(t)(t - t^*)$ in a small time interval after impact and $Y(t^*) = 0$, it follows that one can approximate

$$\delta(t - t^*) \approx |\dot{Y}(t)| \delta(Y). \tag{8}$$

Here, the function $\delta(\cdot)$ must be interpreted as some distribution function such that when applied to a smooth enough function $\phi(t)$, one gets $\int_{-\infty}^{\infty} \phi(s) \delta(s - t) ds = \phi(t^-)$ [15, 17, 29]. In other words, the function $\delta(\cdot)$ in Eq. (8) implies that the velocity is approximated to be just prior to the impact. Note that the conventional interpretation of $\delta(\cdot)$ as a Dirac-delta function implies that $\delta(\cdot)$ takes the value exactly at $t = t^*$ and would lead to difficulties as there would be a discontinuous factor $\dot{Y}|\dot{Y}|$ at $Y = 0$. The transformation in Eq. (8) leads

to modeling the effect of impact as a dissipation term, given by the approximation

$$(1 - e)\dot{Y} \delta(t - t^*) \approx (1 - e)\dot{Y} |\dot{Y}| \delta(Y), \quad \text{given that } |\dot{Y}^+| < |\dot{Y}| < |\dot{Y}^-|. \tag{9}$$

This transformation enables “ignoring” the impact condition. On account of the discontinuity in the velocity, the impulsive damping can be interpreted to occur just before the jump in the velocity and can be justified when $(1 - e)$ is small, i.e., when the coefficient of restitution is close to unity. More discussions on the interpretation of differential operations with non-smooth functions in terms of distributions are available in [15, 29].

Equations (5–9) can be written together in a single equation of the form

$$\begin{aligned} \ddot{Y} - \alpha Y - c\dot{Y} + \beta_0 Y^3 - \beta_1 Y^2 \dot{Y} \\ + \beta_2 Y^4 \dot{Y} + (1 - e)\dot{Y} |\dot{Y}| \delta(Y) \\ = \sigma \operatorname{sgn}(Y) W(t), \end{aligned} \tag{10}$$

where the term $(1 - e)\dot{Y} |\dot{Y}| \delta(Y)$ represents an additional damping term due to impact. When the excitation $W(t)$ is a white noise process, the governing equations of motion represent stochastic differential equations and need to be expressed in the first-order Ito form as

$$\begin{aligned} dY_1 &= Y_2 dt, \\ dY_2 &= (\alpha Y_1 + cY_2 - \beta_0 Y_1^3 + \beta_1 Y_1^2 Y_2 - \beta_2 Y_1^4 Y_2 \\ &\quad - (1 - e)Y_2 |Y_2| \delta(Y_1)) dt \\ &\quad + \sigma \operatorname{sgn}(Y_1) dB(t), \end{aligned} \tag{11}$$

where $dB(t)$ indicates the increments of Brownian motion.

The mirror image Zhuravlev transformation discussed above is approximate and valid only when $(1 - e)$ is small [8] and does not completely exclude the discontinuity in the velocity, except for the case when $e = 1$. The effects of the residual velocity jumps due to impact are incorporated into the governing equations of motion using the Dirac-delta function. However, the term $(1 - e)Y_2 |Y_2| \delta(Y_1)$ takes into account only the localized as well as the approximate description of the energy loss at $Y = 0$. This is reasonably accurate when e is close to unity, i.e. when $(1 - e) \ll 1$. Moreover, for $e \approx 1$, the damping associated with the inelastic impact has a relatively small integral effect due to the factor $(1 - e)$.

3.2 Ivanov transformation

In order to avoid the problem of localized approximate damping associated with the Dirac-delta function in the Zhuravlev transformation, a modified non-smooth transformation of the state variables has been developed by Ivanov [20]. This transformation is applicable for both elastic and inelastic impacts. Here, the state variables (X, \dot{X}) are mapped into the (s, v) space following the transformation

$$X = |s| = s \operatorname{sgn}(s), \quad \dot{X} = R v \operatorname{sgn}(s), \quad (12)$$

where $R = R(s, v) = 1 - k \operatorname{sgn}(s, v)$ and $k = \frac{1-e}{1+e} \in [0, 1)$. The values of s and v are not restricted. This transformation not only completely excludes the velocity jump at impact, but also takes into account the effects of loss of impact energy through damping as well as the conditions of reflection from the barrier. For $R = 1$, the Ivanov transformation can be shown to be equivalent to the Zhuravlev transformation; hence, the Ivanov transformation is more generally known as the Zhuravlev–Ivanov transformation. The Zhuravlev–Ivanov non-smooth transformation has been used to study sdo oscillators with inelastic impacts [9]. Here, the authors have derived the equations of motion as a pair of exact first-order stochastic differential equations, and the corresponding transient probability density functions of the state variables have been estimated using the path-integral method.

Using a similar approach, Eq. (12) can be written in the alternative form as

$$s = X \operatorname{sgn}(s), \quad v = R^{-1} \dot{X} \operatorname{sgn}(s). \quad (13)$$

Taking the time derivative of Eq. (13) and substituting in Eq. (1), the governing equations of motion can be rewritten in terms of the s and v coordinates as

$$ds = Rv, dt, \quad (14)$$

$$dv = \left\{ cv + \beta_1 s^2 v - \beta_2 s^4 v + R^{-1} [\alpha s - \beta_0 s^3] \right\} dt + R^{-1} \sigma \operatorname{sgn}(s) dB(t). \quad (15)$$

Equations (14–15) describe the dynamics of the DVDP vibro-impact oscillator on the barrier-free plane (s, v) , whose values are not restricted. Due to the presence of the signum function, Eq. (15) has a discontinuous right-hand side. However, the solution of these equations is continuous function of time and is differentiable, provided that $sv \neq 0$. The advantage of the

Zhuravlev–Ivanov transformation is that all the conditions at impact are satisfied. At the impact line $s = 0$, the product sv changes sign—say from negative to positive—upon crossing the line. This leads to changes in the corresponding value of R which switches from $(1+e)$ to $(1-e)$. Therefore, the impact condition holds good at the boundary at $X = 0$ and also ensures that the velocity remains continuous in the transformed space.

3.3 Numerical challenges

Even though the discontinuity due to impact in the state space can be removed using the non-smooth coordinate transformations, numerical integration of the governing equations of motion still poses a challenge due to the presence of discontinuities such as the signum function and the Dirac-delta function when Zhuravlev transformation is applied and the signum function only on application of the Ivanov transformation. To bypass these difficulties, the signum function is approximated as [26,37]

$$\operatorname{sgn}(\dot{Y}) = \frac{2}{\pi} \operatorname{atan}(\Theta \dot{Y}), \quad \Theta \gg 1, \quad (16)$$

where Θ is a large number denoting the levels of approximation of the $\operatorname{sgn}(\cdot)$ function. For $\Theta = 10^4$, a good approximation is obtained and the discontinuity of the *signum* function at zero is avoided; see Fig. 2. Additionally, the Dirac-delta function is approximated as a Gaussian probability density function of very low variance. In the numerical calculations, the variances are taken to be of the order of 10^{-3} . Note that since in this study the investigations are limited to impacts

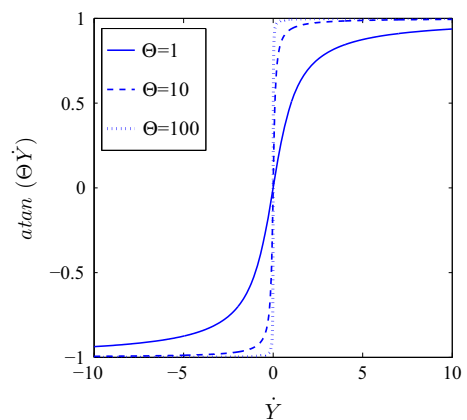


Fig. 2 Approximation of the *signum* function using a continuous function with parameter Θ

with e close to unity, Eq. (10) has been used for the stochastic stability analyses. However, later a comparison of the probability density function obtained for the state variables has been provided to illustrate the differences in accuracy of the results obtained when Ivanov non-smooth transformation is applied vis-a-vis the Zhuravlev transformation.

4 Stochastic bifurcation

Bifurcations in dynamical systems are characterized in terms of dramatic changes in their dynamical behavior leading to topological changes in the phase space. This involves either the birth or destruction of attractors and/or changes in their size and shape in the attractors in the phase space. The stability characteristics of the attractors are estimated by investigating the long-term behavior of the trajectories—an exponential divergence of neighboring trajectories indicates instabilities and is best measured in terms of the Lyapunov exponents (LE) that describe the long-term behavior of the trajectories of the state variables in the phase space. Qualitative changes in the nature of the Lyapunov exponents as the control parameters are varied are indicative of bifurcations.

The response of stochastically excited nonlinear dynamical systems is a random process in time, and the trajectories are accompanied by small fluctuations, which never die down. Hence, the deterministic interpretation of bifurcations needs modifications for the stability analysis of such systems. It has been established in the literature that the stochastically excited systems could undergo two distinct forms of bifurcations: (a) dynamical or D-bifurcations occur when there are drastic topological changes associated with the phase space trajectories, and (b) phenomenological or P-bifurcations are observed when the underlying probabilistic structure of the long-term behavior of the state variables undergoes topological changes. More details on D- and P-bifurcations for the vibro-impact system being studied are discussed in the following sections.

4.1 D-bifurcation analysis

The presence of noise in a dynamical system implies that the state space trajectories inherit the time-varying

fluctuations in the system and hence the Lyapunov exponents associated with the state variable trajectories can only be interpreted in terms of the long-term temporal mean. Assuming $\mathbf{Y}_0(t)$ to be a stable solution for Eq. (10), a small perturbation \mathbf{u} to the trajectory of $\mathbf{Y}_0(t)$ is governed by the linearized equation

$$\dot{\mathbf{u}} = \mathbf{J}(t)\mathbf{u}, \quad (17)$$

where $\mathbf{J} \in \mathfrak{R}^{N \times N}$ is the Jacobian calculated about the reference solution $\mathbf{Y}_0(t)$. Using the principle of Oseledec's multiplicative theorem, the Lyapunov exponents are mathematically defined as

$$\lambda_i = \lim_{t \rightarrow \infty} E \left[\frac{1}{t} \log \frac{\|\mathbf{u}(t)\|}{\|\mathbf{u}(0)\|} \right], \quad (18)$$

where $\{\mathbf{u}(t) : t > 0\}$ are the solution trajectories of the linear differential equations when Eq. (11) is linearized about a reference solution $(Y_1(t), Y_2(t))$ for $t \geq 0$, $\|\cdot\|$ is the Euclidean norm, and $E[\cdot]$ is the expectation operator. Computation of the Lyapunov exponents requires solving for $\mathbf{u}(t)$ which are coupled with Eq. (11) and hence is computationally intensive. This has led to the development of several numerical algorithms, such as Wolf's algorithm [30, 38], where the Lyapunov vectors are approximated using the Gram–Schmidt reorthonormalization algorithm and Wedig's algorithm [35] which uses the principle of Khassminskii's unit projection theorem. It has been shown that irrespective of the algorithm that is used, Wolf's or Wedig's algorithms show similar qualitative analysis of the stability of the system [36]. The largest Lyapunov exponent (LLE) is indicative of the stability of the dynamical system—a negative LLE indicates a stable system and a change in the sign of the LLE reflects a bifurcation. A bifurcation analysis based on the LLE captures the dynamical changes associated with the system and is known as D-bifurcation analysis [2–5].

Computing the LLE from Eq. (11) has obvious difficulties due to the presence of the discontinuous signum function and the inherent numerical issues in estimating the Jacobian. One can approximate the signum function using Eq. (16); however, the gradient function would still be steep and may introduce numerical errors. To validate the numerical computations, an alternative method based on discontinuity mapping is explored. The discontinuity map, coined by Nordmark [27], is a synthesized Poincaré map which is piecewise smooth and is defined locally near the grazing point at

which a trajectory interacts with a discontinuity boundary. Nordmark map provides local decomposition of a Poincare mapping into a sequence of four classes to distinguish between the contributions from the flow and those from the impact process. A general method, based on Nordmark mapping, for the computation of the LE spectrum using Gram–Schmidt orthonormalization for deterministic non-smooth systems, has been presented in [21]. For stochastic systems, a general formulation for estimating the LLE for vibro-impact systems has been developed in [12] using Nordmark mapping and Wedig’s algorithm based on Khasminskii’s unit projection theorem.

For a grazing discontinuity at $X_1 = 0$, this implies that for $X_1 > 0$, the trajectories are continuous and consequently, a small perturbation \mathbf{v} to the trajectory $X_0(t)$ of Eq. (1) is governed by the linearized equation

$$\dot{\mathbf{v}} = \mathbf{J}_1(t)\mathbf{v}, \quad \mathbf{X}_1 > \mathbf{0}, \tag{19}$$

where \mathbf{J}_1 is the Jacobian matrix given by

$$\mathbf{J}_1 = \begin{Bmatrix} 0 & 1 \\ \alpha - 3\beta_0 X_1^2 + 2\beta_1 X_1 X_2 - 4\beta_2 X_1^3 X_2 & c + \beta_1 X_1^2 - \beta_2 X_1^4 \end{Bmatrix}. \tag{20}$$

The approximate discrete map, for the perturbation \mathbf{v} at the time of impact, i.e., $X_1 = 0$, can be constructed using the Nordmark local map [27]

$$\mathbf{v}_k^+ = [\mathbf{D}_{P_c}]_{\mathbf{X}_0(t)} \mathbf{v}_k^-, \quad \mathbf{X}_1 = \mathbf{0}, \tag{21}$$

where \mathbf{D}_{P_c} is a compound map which describes the impact process through the Jacobian matrix

$$\mathbf{D}_{P_c} = \begin{Bmatrix} -e & 0 \\ \frac{(1+e)(\alpha X_{1k} + \beta_0 X_{1k}^3 + \sigma W(t_k))}{X_{2k}} & -e \end{Bmatrix}. \tag{22}$$

The resultant discrete map eliminates the necessity for the Jacobian matrix calculations at the singularity and simplifies the computations. Subsequently, Wedig’s algorithm as discussed above can be applied for estimating the LLE and is defined as

$$\begin{aligned} \lambda_m &= \lim_{t \rightarrow \infty} \frac{1}{t} \log \|\mathbf{v}(t)\| \\ &= \lim_{t \rightarrow \infty} \frac{1}{t} \log \left[\|\mathbf{v}(t)\| \right]_{t \neq t_k} \\ &\quad + \lim_{n \rightarrow \infty} \frac{1}{n} \sum_{k=1}^n \log \left[\|\mathbf{D}_{P_c} S_k^-\| \right]_{t=t_k} \end{aligned} \tag{23}$$

Here,

$$S_i = \frac{v_i}{\sqrt{v_1^2 + v_2^2}}. \tag{24}$$

is obtained by applying Khasminskii’s unit projection. For more details on the derivation of Nordmark Poincare mapping, the reader may refer [27].

A comparison of the LLE estimated using Wedig’s algorithm obtained from Nordmark’s discontinuity map and when the Zhuravlev transformations are used is shown in Fig. 3a, b, for three different values of the restitution coefficient e . The control parameters were taken to be the damping coefficient c in Fig. 3a and linear stiffness coefficient α in Fig. 3b. It can be seen that the estimates of LLE are close in either method, indicating the acceptability of using the Zhuravlev transformed equations with the approximations for the signum function and the Dirac-delta function.

For the parameter regime $-0.15 < c < -0.05$ and $\alpha = -1$, Fig. 3a reveals that the LLE > 0 , indicating that the system is dynamically unstable. However, for the same parameter regimes, an impact-free system shows either small- or large-amplitude oscillations about the origin which is a stable fixed point for the oscillator; see [24]. Putting a barrier at the fixed point prevents the system from converging into it and results in the system losing its stability. Increasing e and thereby reducing energy loss due to impact is seen to have a destabilizing effect on the system dynamics. This type of stochastic instability is therefore called discontinuity-induced instability.

Next, the dynamic stability is investigated with the linear stiffness coefficient α as the bifurcation parameter, when $c = -0.08$. An inspection of Fig. 3b reveals that irrespective of restitution coefficient e , at $\alpha_c \approx 0.5$, the oscillator undergoes D-bifurcations. For barrier-free DVDP oscillator at $\alpha_c \approx 0.5$, the origin becoming unstable is accompanied by the birth of two stable fixed points at $(\pm\sqrt{\alpha/\beta_0}, 0)$; see [24]. Hence, a barrier at origin forces the oscillator to move around one of its fixed point from barrier-free region. Since this fixed point is sufficiently far from zero offset barrier, the impact does not induce instability in the system dynamics.

4.2 P-bifurcation analysis

Stochastically excited dynamical systems additionally undergo P-bifurcations, characterized by changes in the

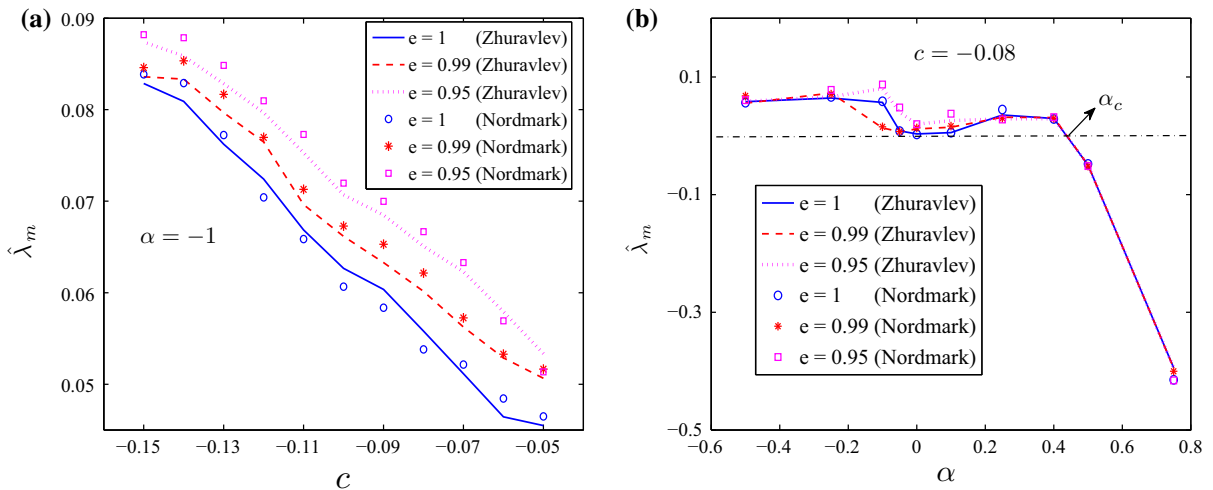


Fig. 3 Estimates of LLE with **a** c and **b** α as bifurcation parameters

probabilistic structure of the stationary joint probability density function (pdf) of the state variables at different parameter regimes. The j-pdf of the state variables is a statistical measure of the time spent by a typical solution in a volume element in the phase space domain and gives an indication of the spatial extent of the stochastic attractor. P-bifurcations are characterized by dramatic changes in the topology of this stochastic attractor space. Since the j-pdf is obtained through a one-point motion and does not explicitly take into account the system dynamics [32], P-bifurcation analysis is essentially a static concept and cannot be related to D-bifurcations. Hence, P-bifurcations is an additional measure that needs to be investigated in stochastic bifurcation analysis.

P-bifurcation analysis provides a qualitative measure for topological variation in the probabilistic structure of stationary j-pdf of the state variables at different parameter regimes. Under Gaussian white noise excitation, the state vector $\mathbf{Y} = [Y_1 \ Y_2]^T$ from Eq. (10) will be Markovian in \mathfrak{R}^2 , and the time evolution of the joint pdf $p(\mathbf{Y}, t | \mathbf{Y}_0, t_0)$ is governed by the Fokker–Planck (FP) equation

$$\begin{aligned} \frac{\partial p}{\partial t} = & -Y_2 \frac{\partial p}{\partial Y_1} - \frac{\partial}{\partial Y_2} \left(\alpha Y_1 + c Y_2 - \beta_0 Y_1^3 \right. \\ & \left. + \beta_1 Y_1^2 Y_2 - \beta_2 Y_1^4 Y_2 - (1 - e) Y_2 |Y_2| \delta(Y_1) p \right) \\ & + \frac{\sigma^2}{2} \frac{\partial^2 p}{\partial Y_2^2}. \end{aligned} \tag{25}$$

Similarly, the FP equation corresponding to Eqs. (14–15) can be shown to be of the form

$$\begin{aligned} \frac{\partial p}{\partial t} = & - \frac{\partial(Rv)p}{\partial s} \\ & - \frac{\partial \left[cv + \beta_1 s^2 v - \beta_2 s^4 v + R^{-1}(\alpha s - \beta_0 s^3) \right] p}{\partial v} \\ & + \frac{\sigma^2}{2} \frac{\partial^2 [R^{-2} p]}{\partial v^2}. \end{aligned} \tag{26}$$

A stationary solution for the joint pdf of displacement and velocity is obtained by letting $\partial p / \partial t = 0$ in either Eqs. (25) or (26) and obtaining a solution for the resultant ordinary differential equation. A numerical solution for the equation is obtained by using a recently developed finite element-based method [23]. The numerical difficulties due to the discontinuity in the FP equation are bypassed by approximating the signum function as in Eq. (16). The Dirac-delta function has been approximated as a Gaussian pdf with mean zero and variance $\approx 10^{-3}$. Once the j-pdf in the transformed plane (Y_1, Y_2) or (r, s) -space is available as a solution of the FP equation, the stationary j-pdf in the original space (X_1, X_2) is obtained using standard transformations, where $X = |Y| = g(Y)$. It can be shown that

$$\begin{aligned} p_{X_1, X_2}(x_1, x_2) &= p_{Y_1, Y_2}(x_1, x_2) + p_{Y_1, Y_2}(-x_1, -x_2) \\ &= 2p_{Y_1, Y_2}(x_1, x_2), \end{aligned} \tag{27}$$

Here, one takes advantage of the symmetry in $p_{Y_1 Y_2}(\cdot)$ about the origin.

5 Numerical results

For the numerical calculations, the parameters in Eq. (1) are taken to be $\beta_0 = 0.5$, $\alpha = -1$, $\beta_1 = \beta_2 = 1$. The damping parameter c , coefficient of restitution e , and the noise intensity σ are taken to be the control parameters which are varied. The variation in e is limited to the range $[0.9-1]$ as for low e values, the Markovian approximation for the response becomes less accurate due to the higher impact losses. For the FE solution of the FP equation, the domain space is discretized using 400×400 quadrilateral elements [23].

To investigate the effect of e on the stability characteristics of the dynamical system, the stationary pdf is computed for the cases $e = 1, 0.99, 0.95$, when $\sigma = 0.1$ and $c = -0.1$. Figure 4a–c shows the j-pdf for these three cases, while Fig. 5a–c shows the corresponding contour plots. Figures 4a and 5a clearly reveal the bistable character of the pdf when $e = 1$; the two stochastic attractors—one representing small-

amplitude oscillations while the other represents large-amplitude oscillations—are clearly visible in the contour plot. At $e = 0.99$, the strength of the attractor at the origin increases while the other weakens. This is indicative of the increasing damping effect due to the inelasticity introduced due to impact losses, and the system has less energy for large-amplitude oscillations. Subsequently, at $e = 0.95$, the attractor for large-amplitude oscillations is destroyed and the system only exhibits small-amplitude oscillations; see Figs. 4c and 5c. These changes are also clearly seen in the marginal pdfs of displacement shown in Fig. 6a–c. These changes in the topological characteristics associated with the stochastic attractors are indicative of P-bifurcation. Interestingly, an inspection of Fig. 5a shows that the LLE does not undergo any sign change on varying e from unity to 0.95, implying that there are no D-bifurcations. This represents a situation where P-bifurcation is observed without being accompanied by a corresponding D-bifurcation.

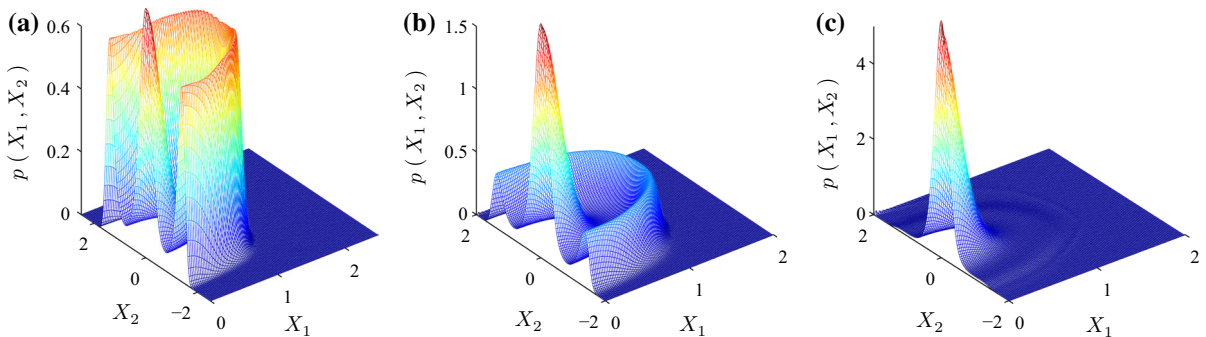


Fig. 4 Stationary joint pdf $p_{X_1 X_2}(x_1, x_2)$; $\sigma = 0.1, c = -0.1$; **a** $e = 1$, **b** $e = 0.99$, **c** $e = 0.95$

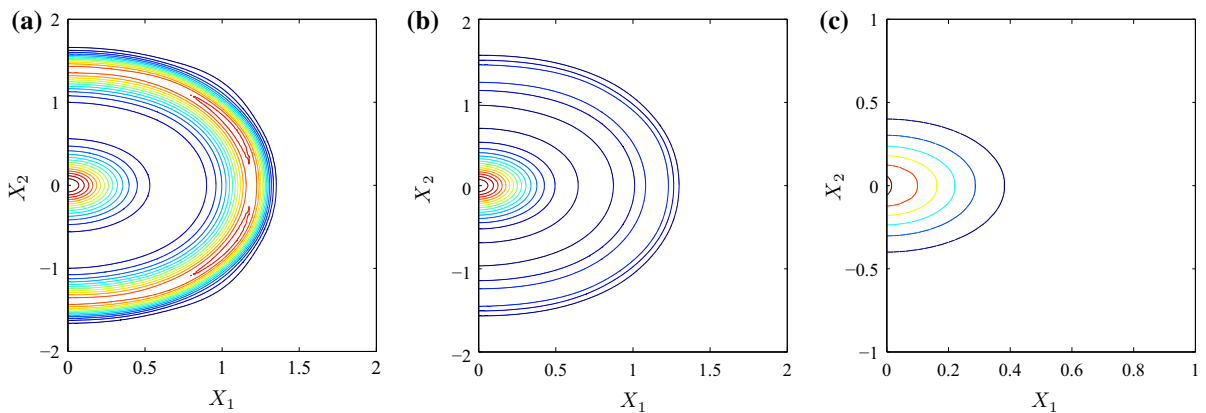


Fig. 5 Contour plots for $p_{X_1 X_2}(x_1, x_2)$; $\sigma = 0.1, c = -0.1$; **a** $e = 1$, **b** $e = 0.99$, **c** $e = 0.95$

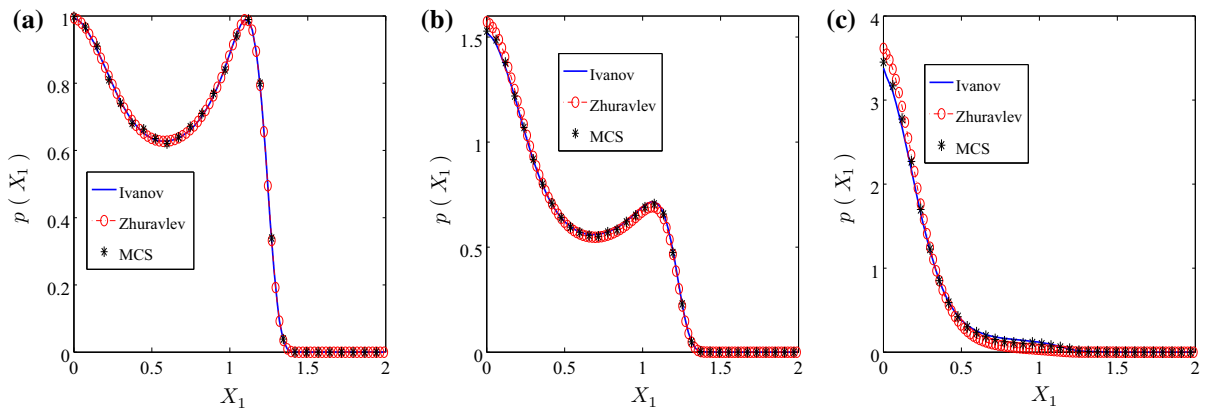


Fig. 6 Marginal pdf of displacement; $c = -0.1, \sigma = 0.1$; **a** $e = 1$, **b** $e = 0.99$, **c** $e = 0.95$

Figure 6a–c also shows a comparison of the estimated marginal obtained when using the Zhuravlev transformation vis-a-vis those obtained using Ivanov transformation. Additionally, the pdf obtained from Monte Carlo simulations (MCS) is also presented. In MCS, the governing equations are numerically integrated, and the corresponding results are treated as the benchmark. Figure 6a shows the marginal pdf when $e = 1$. As can be seen, all the three curves are coincident. This not only illustrates the accuracy of the FE-based solutions of the FP equations, but also highlights that for $e = 1$, the Zhuravlev and the Ivanov transformations coincide as has already been stated earlier. The pdf shown in Fig. 6b is for the case $e = 0.99$ and here too a good agreement between the predictions obtained by the three methods is observed. Figure 6c presents the estimated pdfs when $e = 0.95$. Here, one can see that the predictions obtained from the solution of the FP equation obtained from Ivanov transfor-

mation and MCS are coincident. However, there are slight differences in the predictions obtained from the solution of the FP equation corresponding to the Zhuravlev transformation. Clearly, the difference seems to increase with a decrease in e . This is especially true at the tail regions and is indicative of the loss of accuracy, especially if one is interested in reliability calculations. However, as in this study the focus is on carrying out a stability analysis and identifying the stability boundaries in different parameter regimes, the Zhuravlev transformation-based analysis is not expected to lead to significant errors, especially as the range of e is taken to be limited to close to unity.

Next, considering $e = 0.95$ and $\sigma = 0.1$, the bifurcation characteristics are investigated when $c = -0.05, -0.07$ and -0.11 . Figure 7a–c shows the stationary joint pdf obtained from the solution of the FP equation, while Fig. 8a–c shows the corresponding contour plots. It can be observed that for $c = -0.05$, there

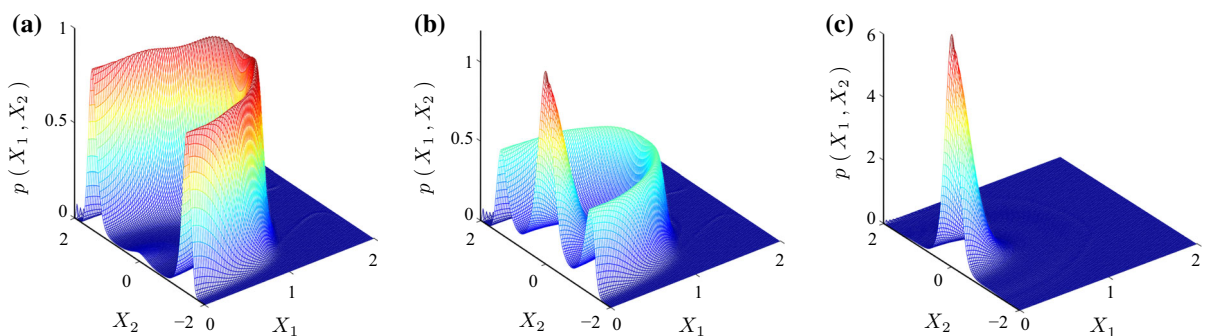


Fig. 7 Stationary joint pdf $p_{X_1 X_2}(x_1, x_2)$; $\sigma = 0.1, e = 0.95$; **a** $c = -0.05$, **b** $c = -0.07$, **c** $c = -0.11$

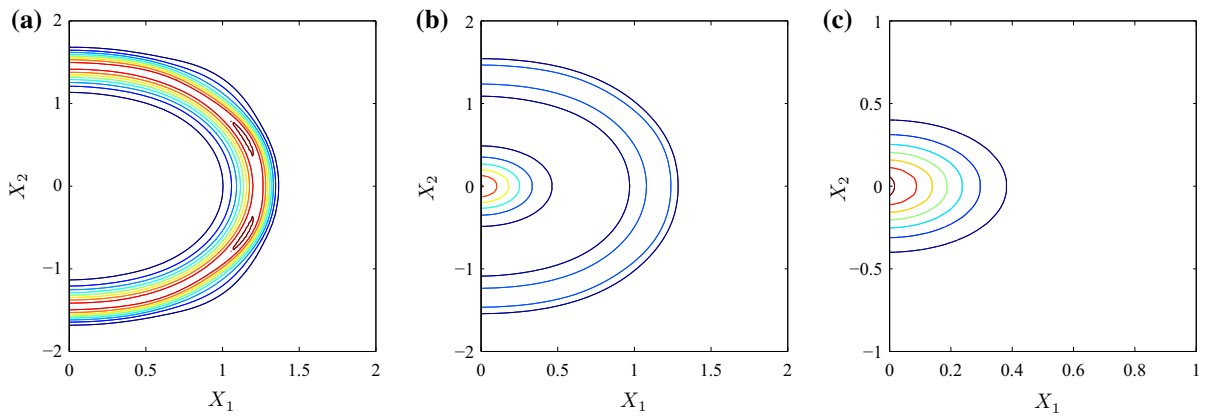


Fig. 8 Contour plots for $p_{X_1 X_2}(x_1, x_2)$; $\sigma = 0.1, e = 0.95$; **a** $c = -0.05$, **b** $c = -0.07$, **c** $c = -0.11$

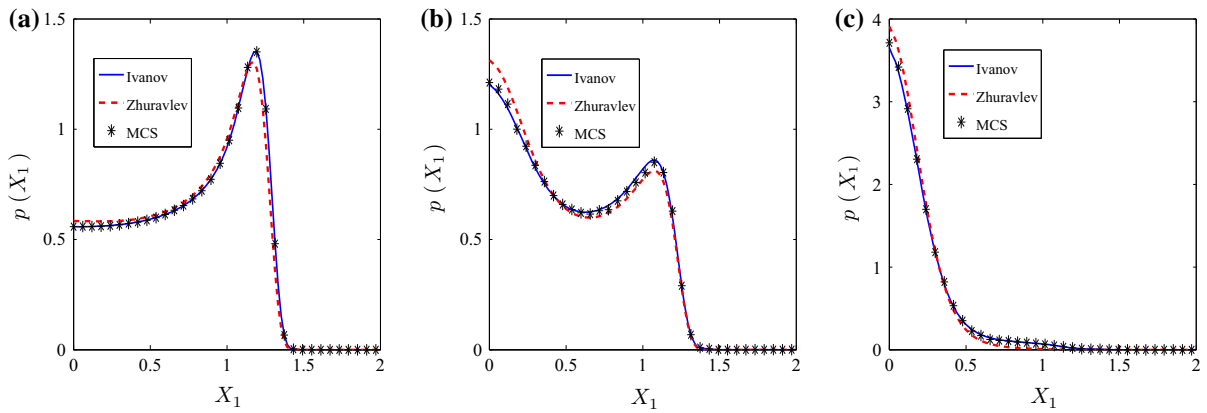


Fig. 9 Marginal pdf of displacement; $\sigma = 0.1, e = 0.95$; **a** $c = -0.05$, **b** $c = -0.07$, **c** $c = -0.11$

exists only one stochastic attractor—characterized by large-amplitude oscillations; see Figs. 7a and 8a. At $c = -0.07$, the birth of a new attractor at the origin is observed while the existing attractor weakens; see Figs. 7b and 8b. On further changing c to -0.11 , it is observed that the attractor associated with the large-amplitude oscillations is completely destroyed and only one attractor around the origin exists. Clearly, a P-bifurcation occurs within this parameter regime. Qualitatively, the effects of increasing the magnitude of the damping parameter c is similar to the effect of reducing e . This is expected as both have the effect of increasing the damping in the system. An inspection of Fig. 3a reveals that the LLE remains positive in this regime, indicating that the phase space trajectories do not undergo any changes and hence P-bifurcation is not accompanied by a D-bifurcation.

Figure 9a–c shows the estimates of the marginal pdf of X obtained from Eqs. (25), (26), and MCS. The errors in the predictions when using the Zhuravlev transformed equations are clearly discernible in all three figures.

Next, the effect of the noise intensity on the behavior of the vibro-impact oscillator is examined. Figure 10a–c presents the stationary joint pdf $p_{X_1 X_2}(x_1, x_2)$ for the system when $c = -0.1, e = 0.99$ for three different values of noise intensity $\sigma = 0.075, 0.1$ and 0.25 . The corresponding contour plots for the joint pdf are shown in Fig. 11a–c. Figures. 10a and 11a clearly show the existence of two stochastic attractors—one corresponding to large-amplitude oscillations and the other corresponding to small oscillations about zero. For $\sigma = 0.075$, the attractor around zero is stronger with, on an average, fewer large-amplitude oscilla-

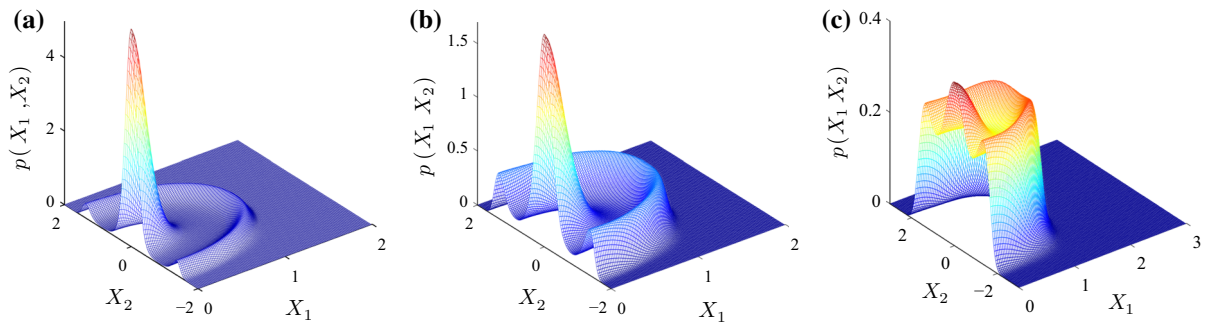


Fig. 10 Stationary joint pdf $p_{X_1 X_2}(x_1, x_2)$; $c = -0.1, e = 0.99$; **a** $\sigma = 0.075$ **b** $\sigma = 0.10$, **c** $\sigma = 0.25$

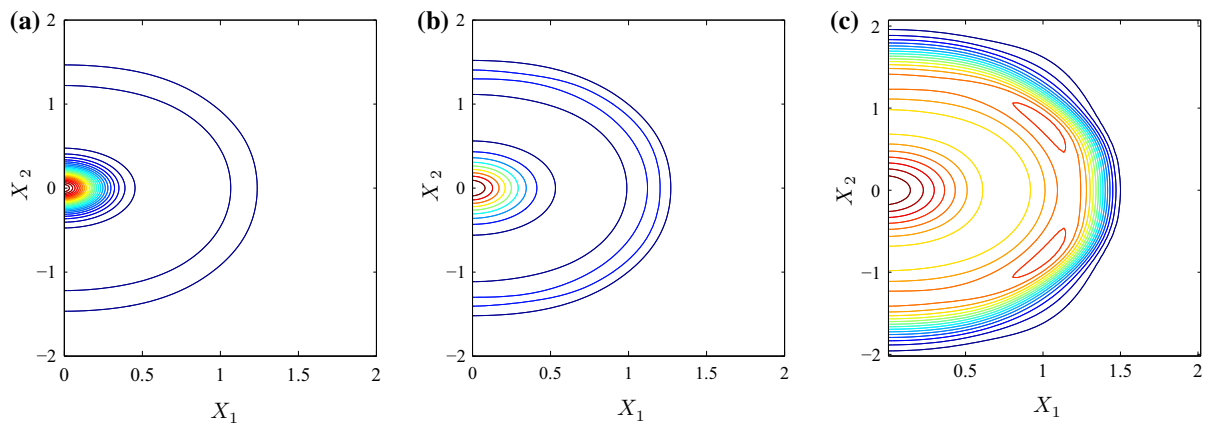


Fig. 11 Contour plots for $p_{X_1 X_2}(x_1, x_2)$; $c = -0.1, e = 0.99$; **a** $\sigma = 0.075$, **b** $\sigma = 0.10$, **c** $\sigma = 0.25$

tions. However, as σ is increased, the attractors are observed to increase in size, and on further increase of the noise intensity, the two attractors are observed to merge together. The physical implication is that higher noise intensity implies larger input energy in the excitations which results in the system being pushed out from one attractor to the other more often.

6 Boundaries of stochastic bifurcation regimes

D-bifurcations are characterized by a sign change in the LLE and the locus in the parameter space where these sign changes occur indicating the boundaries for D-bifurcations. In contrast, P-bifurcation analysis is primarily a qualitative analysis, based on visual inspection of the structure of the pdf of the response. This makes it difficult to define the stability boundaries in terms of P-bifurcations. A quantitative measure based on the

Shannon entropy has been recently proposed in [24] for identifying P-bifurcations quantitatively.

The Shannon’s entropy of $\mathbf{X}(t)$ at time t is defined as

$$H(a, t) = - \int_{-\infty}^{\infty} p(a, t) \log_b p(a, t) da, \tag{28}$$

where b is an arbitrarily chosen logarithmic base, usually taken to be Euler’s number. It has been shown in [28] that under stationary conditions, the entropy flux is proportional to the negative sum of the Lyapunov exponents implying that the entropy changes depend on the phase space contraction and a correction term that depends on the noise strength σ .

Investigations carried out in [24] reveal that the Shannon entropy measure computed from the 1-d pdf obtained for the amplitude process $A(t)$, defined as $A(t) = \sqrt{X_1(t)^2 + X_2(t)^2}$, can be used as a measure to indicate the onset of P-bifurcations. It has been

Fig. 12 Variation in Shannon entropy $H(a)$ with the control parameter; **a** $\sigma = 0.1$ **b** $e = 0.99$; **I** : Ivanov transformation, **Z** : Zhuravlev transformation

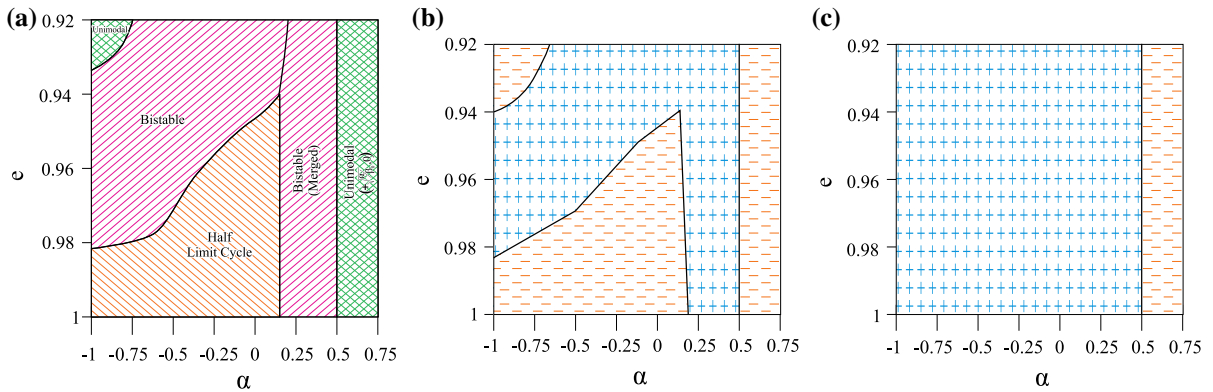
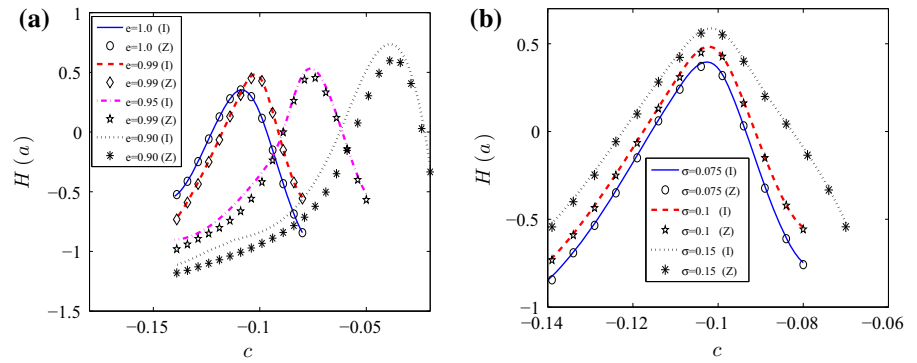


Fig. 13 Identifying stochastic stability regimes for $c = -0.08$ based on **a** qualitative analysis of the joint pdf $p_{X_1 X_2}(x_1, x_2)$ **b** Shannon entropy measure estimated from the pdf of amplitude, $P_A(a)$ and **c** sign of the largest Lyapunov exponent

observed that $H(a) < 0$ in parameter regimes characterized by a single stochastic attractor, and $H(a) > 0$ otherwise. For the vibro-impacting oscillator being studied in this paper, P-bifurcations are characterized by the onset of bistability with the birth of a new attractor, a parameter regime when both attractors exist with one weakening and the other strengthening and eventually the destruction of the existing attractor. Figure 12a–b shows the variation in $H(a)$ with c being the control parameter for different values of e . It is observed that for a specified e and low values of c , the Shannon entropy $H(a) < 0$. As the magnitude of c is gradually increased, the system exhibits bistable behavior with the presence of two stochastic attractors. In this regime, $H(a) > 0$. On further changes in c , one of the attractors is destroyed and the system once again reverts back to a single stochastic attractor, though usually a different one. In these regimes, $H(a) < 0$ once again. This is illustrated by looking at the results corresponding to $e = 0.95$ and comparing with the results shown in Fig. 8a–c. The effects of noise intensity parameter, σ , on

Shannon entropy are shown in Fig. 12b. It is clearly seen that an increase in noise intensity is accompanied by an increase in the Shannon entropy measure. This also implies that the associated disorder with the system is higher and accounts for the higher Shannon entropy observed. These results indicate that one can define a new quantitative measure to indicate P-bifurcations as when $H(a)$ undergoes a sign change. It is interesting to note that the Shannon entropy measure computed with respect to the joint pdf $p_{X_1 X_2}(x_1, x_2)$ do not reveal such characteristic features. Interestingly, the differences in the predictions when using Zhuravlev transformed equations vis-a-vis Ivanov transformed equations can be clearly seen: It is observed that the differences increase as e decreases from unity.

Next, a global parametric study is undertaken for identifying the stability regimes in the $\alpha - e$ parameter space for the noisy DVDP vibro-impact oscillator, using three different methods. Figure 13a shows the different regimes identified based on visual inspection of the joint pdfs computed from the solution of the FP

equation; this is the traditional P-bifurcation analysis based on qualitative changes in the structure of the joint pdf. Figure 13b shows the bifurcation diagram using the Shannon entropy definition $H(a)$ based on $p_A(a)$. This is a quantitative approach to P-bifurcation analysis. The bifurcation diagram shown in Fig. 13c is obtained based on D-bifurcation analysis from the computation of the LLE. The parameter space in Fig. 13a is mainly subdivided into three different zones, the nomenclature of which is as follows: (i) half limit cycle—the only attractor is the limit cycle where one obtains large-amplitude oscillations in the positive half space (due to impact); (ii) unimodal—only one attractor exists at the fixed point, characterized by small-amplitude oscillations; and (iii) bistable—both stochastic attractors—large-amplitude and small-amplitude oscillations exist simultaneously. It must be emphasized here that the boundaries of these zones do not have sharp demarcations, and these are based on qualitative analysis based on visual inspection of the j-pdf. On the other hand, Fig. 13b is divided into regimes based on the sign of $H(a)$; $H(a) > 0$ in the regions marked by the plus signs. It is observed that there are very close similarities between Fig. 13a, b. The parameter ranges where $H(a) > 0$ in Fig. 13b correspond to regimes where the system exhibits bistability. This indicates the usefulness of the Shannon entropy approach in quantifying P-bifurcations. The demarcation of the regimes in Fig. 13c is based on the sign of LLE. A comparison of the bifurcation diagrams in Fig. 13c with either Fig. 13a or b clearly indicates that D- and P-bifurcations need not occur simultaneously in certain parameter ranges.

7 Concluding remarks

Investigations on the stochastic bifurcations for a DVDP vibro-impact oscillator subjected to Gaussian white noise excitation have been carried out. Damping and stiffness coefficients, noise intensity, and coefficient of restitution have been taken to be the control parameters. The presence of impact introduces complexities in the equations of motion which leads to difficulties in the numerical analysis. The equations of motion and the constraint equations are recast into a single equation by adopting non-smooth transformations, such as the Zhurvalev transformation and the more accurate Ivanov transformations. The discontinuities in the resultant equations of motion that poses numerical

difficulties are bypassed by adopting approximations. The accuracy of these approximations has been validated by comparing the largest Lyapunov exponent estimated using Nordmark discontinuity mapping. The estimated largest Lyapunov exponents have been used for carrying out D-bifurcation analysis. The locus of the parameters at which the sign of the LLE changes indicates the dynamical stability boundaries. P-bifurcation analysis has been carried out by solving for the stationary probability density function of the state variables from the corresponding Fokker–Planck equation using a finite element-based approach. A newly developed quantitative measure based on the Shannon entropy associated with the amplitude process has been used to identify the onset of P-bifurcations. A global parametric study has been carried out to identify the stochastic stability regimes based on visual inspection of the pdf of the state variables, the sign of the Shannon entropy measure, and the sign of the largest Lyapunov exponent. The Shannon entropy-based approach is shown to identify the stability boundaries similar to those identified based on visual qualitative inspections. Moreover, it was shown that D- and P-bifurcations need not occur simultaneously at certain parameter ranges. The numerical results presented in this paper are only representative of extensive studies that have been carried out.

References

1. Arecchi, F., Badii, R., Politi, A.: Generalized multistability and noise-induced jumps in a nonlinear dynamical system. *Phys. Rev. A* **32**(1), 402–408 (1985)
2. Arnold, L.: *Random Dynamical Systems*. Springer, New York (1998)
3. Arnold, L., Crauel, H.: *Random dynamical systems*. *Lect. Notes Mat.* **1486**, 1–22 (1991)
4. Arnold, L.: Sri Namachchivaya, N., Schenk-Hoppe, K.R.: Toward an understanding of stochastic hopf bifurcation: a case study. *Int. J. Bifurc Chaos* **6**(11), 1947–1975 (1996)
5. Baxendale, P.H.: A stochastic hopf bifurcation. *Probab. Theory Rel. Fields* **99**, 581–616 (1994)
6. Davies, H.G.: Random vibrations of a beam impacting stops. *J. Sound Vib.* **68**(4), 479–487 (1980)
7. Di Bernardo, M., Nordmark, A., Olivar, G.: Discontinuity-induced bifurcations of equilibria in piecewise smooth and impacting dynamical systems. *Physica D* **237**, 119–136 (2008)
8. Dimentberg, M.: *Statistical Dynamics of Nonlinear and Time-Varying Systems*. Research Studies Press, Taunton (1988)

9. Dimentberg, M., Naess, A., Gaidai, O.: Random vibrations with strongly inelastic impacts: response pdf by pi method. *Int. J. Nonlinear Mech.* **44**, 791–796 (2009)
10. Dimentberg, M.F., Iourtchenko, D.V.: Random vibrations with impacts: a review. *Nonlinear Dyn.* **36**(2–4), 229–254 (2004)
11. Dimentberg, M.F., Menyailov, A.: Response of a single-mass vibroimpact system to white noise random excitation. *ZAMM J. Appl. Math. Mech.* **59**(12), 709–716 (1979)
12. Feng, J., Xu, W.: Analysis of bifurcation for nonlinear stochastic non-smooth vibro impact systems via top Lyapunov exponent. *Appl. Math. Comput.* **213**, 577–586 (2009)
13. Feng, J., Xu, W., Wang, R.: Stochastic response of vibro impact Duffing oscillator excited by additive gaussian noise. *J. Sound Vib.* **309**(3–5), 730–738 (2008)
14. Feng, J.Q., Xu, W., Rong, H.W., Wang, R.: Stochastic response of Duffing?van der pol vibro impact system under additive and multiplicative random excitation. *Int. J. Non-Linear Mech.* **44**(1), 51–57 (2009)
15. Filippov, A.F.: *Differential equations with discontinuous righthand sides*. Kluwer Academic Publishers, Berlin (1988)
16. Huang, Z.L., Liu, Z.H., Zhu, W.: Stationary response of multi degree-of-freedom vibro-impact system under white noise excitations. *J. Sound Vib.* **275**(1–2), 223–240
17. Ibrahim, R.: Recent advances in vibro-impact dynamics and collision of ocean vessels. *J. Sound Vib.* **333**, 5900–5916 (2014)
18. Ibrahim, R.A.: *Vibro-Impact Dynamics Modeling. Mapping and Applications*. Springer, New York (2009)
19. Iourtchenko, D.V., Song, L.L.: Numerical investigation of a response probability density function of stochastic vibroimpact systems with inelastic inputs. *Int. J. Non-Linear Mech.* **41**(3), 447–455 (2006)
20. Ivanov, A.P.: Impact oscillations: linear theory of stability and bifurcations. *J. Sound Vib.* **178**(3), 361–378 (1994)
21. Jin, L., Lu, Q., Twizell, E.H.: A method for calculating the spectrum of lyapunov exponents by local maps in non-smooth impact vibrating systems. *J. Sound Vib.* **298**, 1019–1033 (2006)
22. Kim, S., Park, S.H., Ryn, C.: Noise-enhanced multistability in coupled oscillator systems. *Phys. Rev. Lett.* **78**, 1616–1619 (1997)
23. Kumar, P., Narayanan, S., Gupta, S.: Finite element solution of Fokker?Planck equation of nonlinear oscillators subjected to colored non-gaussian noise. *Probab. Eng. Mech.* **38**, 143–155 (2014)
24. Kumar, P., Gupta, S.: Investigations on the bifurcation of a noisy Duffing–van der Pol oscillator. *Probab. Eng. Mech.* (accepted)
25. Luo, G.W., Chu, Y.L., Zang, Y.L., Zang, J.G.: Double Neimark?Sacker bifurcation and torus bifurcation of a class of vibratory systems with symmetrical rigid stops. *J. Sound Vib.* **298**(4), 154–179 (2006)
26. Narayanan, S., Jayaraman, K.: Chaotic vibration in a non-linear oscillator with coulomb damping. *J. Sound Vib.* **146**(1), 17–31 (1991)
27. Nordmark, A.B.: Non-periodic motion cause by grazing incidence in an impact oscillator. *J. Sound Vib.* **145**, 279–297 (1991)
28. Phillis, Y.A.: Entropy stability of continuous dynamic system. *Int. J. Control* **35**, 323–340 (1982)
29. Pilipchuk, V.: Non-smooth spatio-temporal coordinates in nonlinear dynamics. <http://arxiv.org/pdf/1101.4597v1.pdf> (2013)
30. Ramasubramanian, K., Sriram, M.S.: A comparative study of computation of lyapunov spectra with different algorithms. *Physica D* **139**, 72–86 (2000)
31. Rong, H., Wang, X., Xu, W., Feng, T.: Resonant response of a non-linear vibro impact system to combined deterministic harmonic and random excitations. *Int. J. Non-Linear Mech.* **45**, 474–481 (2010)
32. Schenk-Hoppe, K.R.: Bifurcation scenario of the noisy Duffing stochastic-Van der Pol oscillator. *Nonlinear Dyn.* **11**, 255–274 (1996)
33. Namachchivaya, N.S., Park, J.: Stochastic dynamics of impact oscillators. *ASME J. Appl. Mech.* **72**(6), 862–870 (2005)
34. Wagg, D., Bishop, S.R.: Chatter, sticking and chaotic impacting motion in a two degree of freedom impact oscillator. *Int. J. Bifurc. Chaos* **11**(1), 57–71 (2001)
35. Wedig, W.: Dynamic stability of beams under axial forces-lyapunov exponents for general fluctuating loads. In: Kr-ig, W. (ed.) *Proceedings Eurodyn'90, Conference on Structural Dynamics*, vol. 1, pp. 57–64 (1990)
36. Wei, J., Leng, G.: Lyapunov exponent and chaos of Duffing's equation perturbed by white noise. *Appl. Math. Comput.* **88**, 77–93 (1997)
37. Wei, S.T., Pierre, C.: Effects of dry friction damping on the occurrence of localized forced vibration in nearly cyclic structures. *J. Sound Vib.* **129**, 397–416 (1989)
38. Wolf, A., Swift, J.B., Swinney, H.L., Vastano, J.A.: Determining lyapunov exponents from a time series. *Physica D* **16**, 285–317 (1985)
39. Zhu, H.T.: Stochastic response of vibro-impact Duffing oscillator under eternal and parametric gaussian white noises. *J. Sound Vib.* **333**, 954–961 (2014)
40. Zhuravlev, V.F.: A method for analyzing vibro-impact systems by means of special functions. *Mech. Solids* **11**, 23–27 (1976)